Challenging Glass Conference Proceedings – Volume 10 – June 2026 – Louter, Bos & Belis (Eds.)
International Conference on the Architectural and Structural Application of Glass
Challenging Glass Conference 10 – 15-17 June 2026 – TU Delft – The Netherlands

AI-Based Crack Propagation Analysis in Structural Glazing Joints under Cyclic Shear Loading

Stefan Wenzel [a], Paul Müller [a], Christian Schuler [a]

a Hochschule München University of Applied Sciences, Institute for Material and Building Research
stefan.wenzel@hm.edu, mueller.paul@hm.edu, christian.schuler@hm.edu

Abstract

This study presents an AI-based methodology for the quantitative evaluation of crack propagation in cyclically loaded thick-layer silicone adhesive joints used in structural glazing systems. Experimental shear tests under low cycle fatigue loading were recorded with a DSLR and analyzed using a convolutional neural network for crack detection and segmentation. A dedicated dataset was generated from video frames and annotated to capture varying crack geometries and substrate positions. Real-time object detection-based segmentation models were trained and systematically optimized through hyperparameter tuning. To address deformation-induced crack distortion, a linear back-calculation was implemented to transform detected crack geometries into an undeformed reference state. This enables the extraction of normalized crack metrics independent of instantaneous deformation. The automated measurements were validated against manual reference evaluations, showing reproducible accuracy across multiple specimens. Increasing input resolution was associated with improved geometric agreement, while training stability depended on an appropriate balance of model complexity. The proposed approach extends conventional experimental evaluation by enabling continuous, image-based crack assessment throughout cyclic loading. This provides a basis for the future evaluation of adhesive joint performance under low-cycle fatigue conditions while accounting for the actual crack propagation behavior.

Keywords

Structural Glazing, Thick-Layer Adhesive Joints, Crack Propagation, Seismic Loading, Deep Learning-Based Image Analysis

Article Information

- Digital Object Identifier (DOI): 10.47982/cgc.10.721
- Published by Challenging Glass, on behalf of the author(s), at Stichting OpenAccess.
- Published as part of the peer-reviewed Challenging Glass Conference Proceedings, Volume 10, June 2026, 10.47982/cgc.10
- Editors: Christian Louter, Freek Bos & Jan Belis

1. State of the art

1.1. Structural-Glazing

The architectural design of modern city centers is characterized by delicate and slender secondary load-bearing structures. Facade constructions are particularly notable in this context, as their load-bearing structure remains largely invisible to the observer and the load transfer mechanism is not immediately evident, an essential design characteristic with significant aesthetic impact. In order to minimize the visible width of load-bearing elements in glass constructions, Structural Glazing Systems (SG) are predominantly used. In these systems, the glazing is connected to a usually concealed secondary supporting structure by means of adhesive joints. However, this construction method places high demands on the adhesives: on the one hand, they must ensure long-term load-bearing capacity; on the other hand, the silicones used exhibit a low modulus of elasticity and complex mechanical behavior, resulting in a demanding design basis.

Previous investigations (Hagl 2007; Müller et al. 2024; Bues et al. 2019; Bucak and Hagl 2006) have already proposed design concepts and verification methods. They demonstrated that even the purely static design of silicone adhesive joints involves a high degree of complexity. In addition to static loading, SG joints must also withstand cyclic actions on high load levels, such as those caused by seismic ground accelerations in some regions. Such earthquake loads lead to complex structural responses within the overall load-bearing system.

1.2. Investigations of Structural Glazing Facades under Seismic Scenarios

Experimental studies by (Müller et al. 2024) examined the load-bearing behavior of thick-layer adhesive joints in structural glazing applications under low-cycle fatigue loading to simulate seismic action. The results showed that the adhesive joints exhibit ductile and comparatively well-predictable failure behavior under cyclic loading. The residual performance of SG joints after seismic low-cycle fatigue loading was investigated in (Müller et al. 2025b), showing predictable performance after partial loading. The seismic ground motion loading on SG joints in glass and facade constructions was analyzed in (Müller et al. 2025a).

In experimental investigations on the behavior of SG joints under seismic loading, the cyclic load-bearing behavior of SG joints subjected to shear was analyzed. The objective was to determine the influence of various parameters on the load-bearing and failure behavior of the adhesive joints. Particular emphasis was placed on the joint geometry (12 × 12 mm and 8 × 24 mm). In addition, the loading frequency was varied, as silicones exhibit different load-bearing capacities depending on the loading rate (Huba and Bojtos, n.d.; Roos et al. 2022; (Wei et al. 2023). The investigations were conducted under both force-controlled and displacement-controlled conditions. The stress ratio was examined for $R = -1$ and $R = 0$, showing no significant influence on cyclic load-bearing capacity.

The observed stiffness degradation can be attributed to the Mullins effect and material-induced micro-damage. Force-controlled tests revealed a continuous increase in deformation with a plateau similar to creep behavior before sudden failure occurred. In contrast, displacement-controlled tests showed a gradual stress reduction and a soft failure mode. With increasing load amplitude, the damage fraction per cycle increased, which is characteristic of fatigue behavior.

Overall, it was found that low cycle fatigue produces a predictable influence pattern on silicone adhesive joints. This enables a reliable prediction of load-bearing and failure behavior under cyclic loading and provides initial design principles for applications in seismic-prone scenarios (Müller et al.

2024). The strength parameters of SG joints can be evaluated based on the recorded force-displacement hysteresis curves. However, for a more advanced assessment of the damage state, the question arises regarding the actual crack behavior in the failure scenario.

1.3. Object Detection in Image Data Using a Neural Network

The use of artificial intelligence (AI) has been proven to increase the efficiency of numerous tasks in civil engineering. In particular, projects on damage detection based on imaging techniques have shown promising results (Flotzinger et al. 2024; Jahangir et al. 2025; Lee et al. 2023). A key role in this context is played by Convolutional Neural Networks (CNNs). These artificial neural networks are inspired by the biological nervous system and consist of layers of computational operations that can be adjusted and controlled through weights, activation functions (mapping of the input), and bias terms (flexibility parameters for adaptation). For image processing, pixel values across color channels are transformed into tensors, resulting in a numerical representation of the image data.

CNNs are particularly suitable for image analysis because they use convolution operations (kernels, typically 2×2, 3×3 or 5x5 matrices) to extract relevant features such as edges or structural patterns. This enables feature extraction and the assignment of visual characteristics to specific objects. Based on small distinctive visual features, the network can infer the presence of an object and perform identification or prediction tasks (Paaß and Hecker 2020).

Training data for AI model development are usually predefined manually. In the annotation process, objects are delineated within images by assigning coordinates. Based on these annotated datasets, the network learns to detect specific objects or damage patterns and to evaluate their occurrence probabilistically. Pooling operations condense the extracted features, emphasizing distinctive characteristics such as edges or color gradients while reducing data dimensionality. Although the mathematical foundations of convolution and pooling are comparatively simple, the multilayered architecture results in high computational demands and enables powerful object detection in complex image data (Sonnet 2022; Paaß and Hecker 2020; Haghsheno et al. 2024; Lei et al. 2012).

The schematic representation in Fig. 1 illustrates how relevant features are extracted from input images through convolution operations during the learning process. Subsequently, pooling operations compress the feature representation by highlighting essential structures and reducing the data volume. For further processing, the multidimensional tensor is transformed into a one-dimensional vector through flattening. Based on this representation, the softmax function computes probability values between 0 and 1. This normalized exponential function provides the probability of object assignment within the image (Paaß and Hecker 2020).

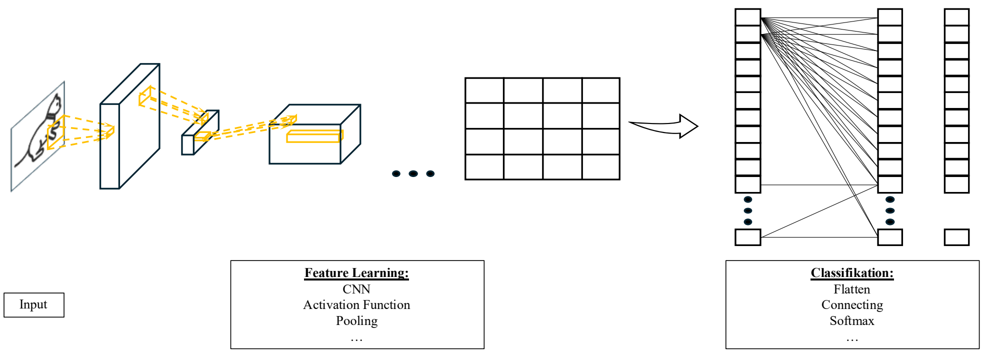

Fig. 1: Schematic representation of the learning process of a CNN.

During the computational process within a neural network, successive forward passes through the layers aim to produce a high output probability corresponding to the given input. In this way, the network is trained to generate probabilistic predictions that result from a specific computational propagation through the model.

The objective is that, for an input such as Object 1, the output layer assigns the highest possible probability to Object 1. The discrepancy between the predicted probability and the true label is quantified using a loss function, such as cross-entropy or mean squared error, in order to measure learning progress or degradation.

1.4. Methodological objective

The objective of this study is to apply neural networks for the quantitative assessment of crack propagation in cyclically loaded SG joints. Within the scope of this work, the fundamental application potential, functionality, and robustness of the developed evaluation methodology are examined. Beyond the mere detection of a crack, particular emphasis is placed on assessing the achievable geometric accuracy in comparison to the actual image data. A positive evaluation of applicability requires that the automated analysis achieves at least comparable or reproducibly more stable accuracy than human interpretation. Furthermore, this work aims to enable a detailed analysis of crack growth behavior over the entire course of the experimental program.

2. Practical Experimental Procedure

The crack propagation investigations presented in this study build upon the material properties of silicones under seismic loading examined in (Müller et al. 2025b). The fatigue behavior was recorded and documented under various loading scenarios using a hydraulic testing machine. The investigations were carried out with variations in joint geometry. The cyclic shear loading was introduced into the material as illustrated in Figure 2.

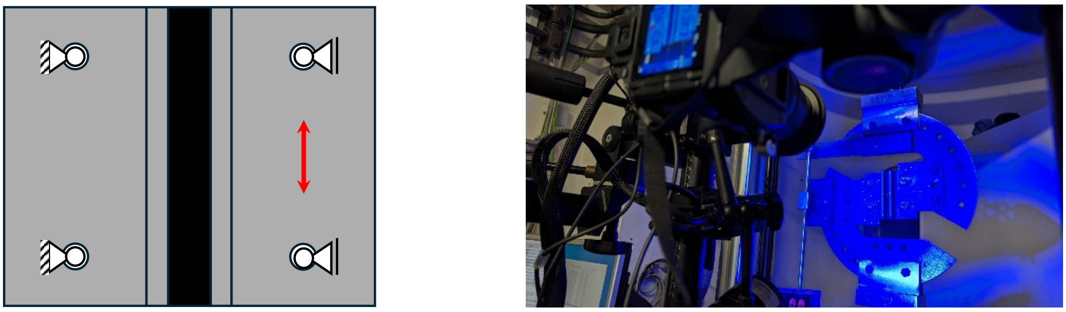

(a) (b)

Fig. 2: (a) Static System of the Shear Tests; (b) Experimental Setup of the Cyclic Material Testing.

To determine the material parameters of the test series, static shear tests were conducted in advance. At approximately 70% of the applied maximum deformation, an initial slight reduction in stiffness was observed due to the onset of cracking between Substrate A and Substrate B. After the crack had propagated to the opposite side of the initial crack initiation zone, the load could be further increased, with the material properties largely corresponding to those prior to crack initiation. As shown in Figure 3, the derivative of the force-displacement curve indicates that crack initiation in the silicone occurs within the deformation range of approximately 11 mm to 14 mm.

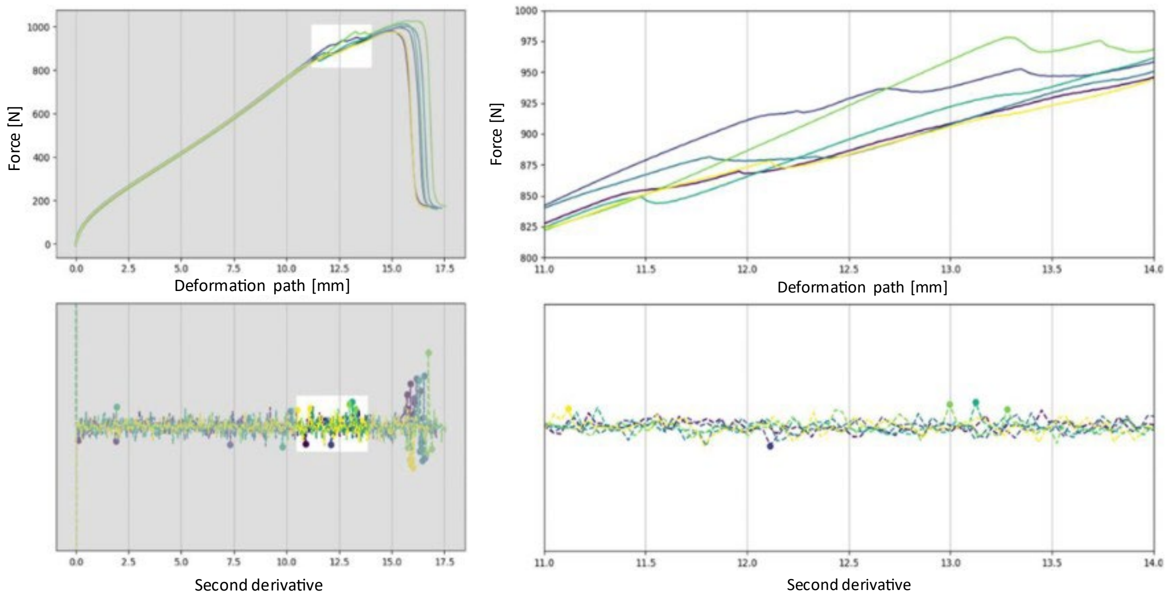

Fig. 3: Force–Displacement Diagram of a Static Test for the Determination of Material Parameters.

The tensile tests revealed an effect that raised the need for a more detailed investigation of crack behavior. Crack characteristics could serve as an additional parameter in the assessment of structural glazing SG joints. By precisely determining crack propagation properties, the experimental investigations can be further extended and refined.

3. Evaluation Methodology

3.1. Training Data: Generation, Preprocessing, and Validation

To develop a model for the automated evaluation of crack growth in shear tests under cyclic loading, it was necessary to create a specialized dataset parameterized to the specific task. For this purpose, individual frames were extracted from video recordings of the experiments. It was essential to cover the widest possible range of crack geometries. Due to the high deformability of silicones and the substrate-dependent crack propagation behavior, a large variety of geometric configurations and visual appearances occurs. Fig. 4a shows a slight deformation in which the crack geometry is partially concealed behind the substrate in the recorded image. In Fig. 4b, crack initiation occurs at the center of the SG joint, and the crack flanks are distorted due to deformation, resulting in a wide crack opening. In Fig. 4c, the strong deformation makes the crack geometry identifiable only by the crack flank on the right side of the crack. By employing a Convolutional Neural Network (CNN), these diverse features relevant to the detection task can be learned, thereby increasing predictive capability and improving robustness against false-positive detections.

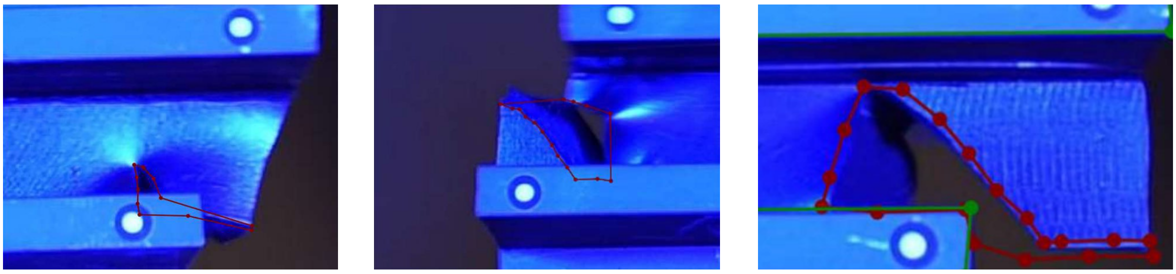

(a) (b) (c)

Fig. 4: (a) Slightly Closed Crack under Low Deformation; (b) Crack Initiation at the Center of the Adhesive Joint, Crack Tip Not Visible; (c) Highly Deformed Crack with Distorted Crack Geometry

The dataset comprised 1228 training images and 481 validation images and was annotated with two labels, the crack in its various manifestations and the respective substrates. For object detection, a YOLO-based neural network was trained. In addition, an RT-DETR model was implemented to systematically compare the performance of both architectures. Hyperparameter tuning was carried out to optimize the models. The configurations were adjusted in such a way that the influence of imaging conditions on detection accuracy could be specifically evaluated. Training was conducted in increments of 100 epochs to enable continuous monitoring and comparison of training progress.

Table 1: Applied Hyperparameters.

Model Designation	Model Scaling (Network size)	Epochs	Resulution
Model_1	YOLOv8_medium	5x100	2048ppx
Model_2	YOLOv8_medium	4x100	1024ppx
Model_3	YOLOv11_extralarge	5x100	2048ppx
Model_4	RT-DETR_medium	3x100	1024ppx

When comparing training runs of different model configurations and network architectures (see Fig. 5), the primary focus was placed on the stability of the precision and recall values. Due to the largely homogeneous imaging conditions of the experiments, the validation loss is less informative than in typical application scenarios, as the model does not need to generalize to highly varying or domain-shifted data. As illustrated in Fig. 5, the main challenge lies in the reliable detection and delineation of crack contours rather than in distinguishing color values or color combinations. Model evaluation was therefore primarily based on segmentation performance, particularly mAP50–95 (M) and Recall (M), since these metrics most reliably reflect the quality and completeness of crack detection.

The evaluation of the hyperparameter tuning indicates that models based on the YOLOv8 architecture with a segmentation task, as well as the real-time detection model, achieved the best performance metrics. In particular, the YOLOv8 model with medium network size and an input resolution of 1024 px delivered significantly more stable and higher values in precision, recall, and mAP50–95 than the YOLOv11 model with a larger architecture and an input resolution of 2048 px.

A further increase in input resolution did not improve performance but instead destabilized the training process. This was reflected in fluctuating metrics and reduced generalization capability. The results suggest that, for the present task, maximum model complexity is not decisive; rather, a balanced ratio between resolution, network size, and feature extraction is critical. This implies that high-resolution imaging requires corresponding adjustments in kernel sizes and feature extraction mechanisms. Due to the largely homogeneous color scheme of the experimental setup, visual features are differentiated primarily through geometric properties rather than color contrasts. Consequently, areas with similar color values may increase uncertainty in feature assignment.

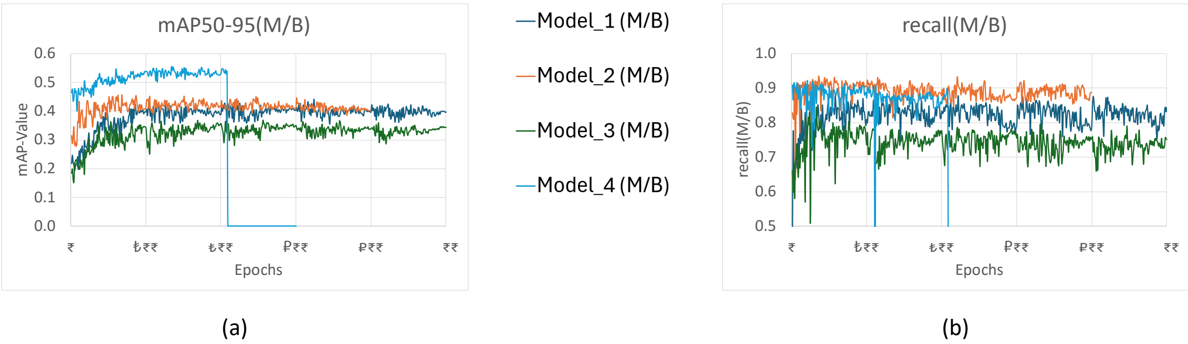

Fig. 5: (a) Performance Metrics mAP50-95(M/B); (b) Performance Metrics recall(M/B).

Stepwise training of the models allows the optimal training state to be identified on an epoch basis and enables the targeted selection of the model exhibiting the most stable and highest-performing metrics. In subsequent analyses, the RT-DETR architecture was not further considered, as training showed clear destabilization from approximately epoch 200 onward. Moreover, the model is primarily designed for real-time bounding-box detection and is not optimized for the present segmentation task.

3.2. Assignment of Classification Results to Experimental Events

A probability-based artificial intelligence model for detection or segmentation does not implicitly differentiate predictions according to semantic positions, labels, or functional meanings in its output. Therefore, an explicit assignment of detected or segmented classes to defined image positions is required within the evaluation process. The defined regions are illustrated in Fig. 6. Prior to the actual analysis, a region-based query is performed to define the image areas in which classifications may occur. On this basis, position-dependent assignments and geometric relationships can be determined, which are necessary for the subsequent analysis of the task.

Fig. 6: Definition of Regions.

The definition of the upper substrate region forms the basis for normalizing the measured crack length. On this basis, it is possible to determine comparable, normalized crack lengths in the evaluation, regardless of the selected image resolution or model size. To further process the information obtained from imaging, a conversion factor is introduced that enables the transformation of pixel values into a percentage-based unit. This allows known reference lengths to be used to convert pixel-based measurements into the desired physical units.

$$k_{norm} = \frac{x_{2,us} - x_{1,us}}{100\%} \quad [\frac{px}{\%}] \tag{1}$$

k_{norm}	=	Conversion factor
$x_{2,us}$	=	Upper substrate area, right corner
$x_{1,us}$	=	Upper substrate area, left corner

In the subsequent evaluation step, the centroid of the corresponding bounding boxes is determined in relation to the segmentation mask. The calculated coordinates are then matched with the previously defined image regions. In this way, each detection or segmentation can be clearly assigned to a specific position and linked to the information relevant for further analysis. The overall evaluation approach and the underlying analysis scheme are illustrated in Fig. 7. Furthermore, by associating spatial coordinates with the recorded data, temporal events such as deformation, degree of deformation, and initiation time within the experiment can be systematically assigned.

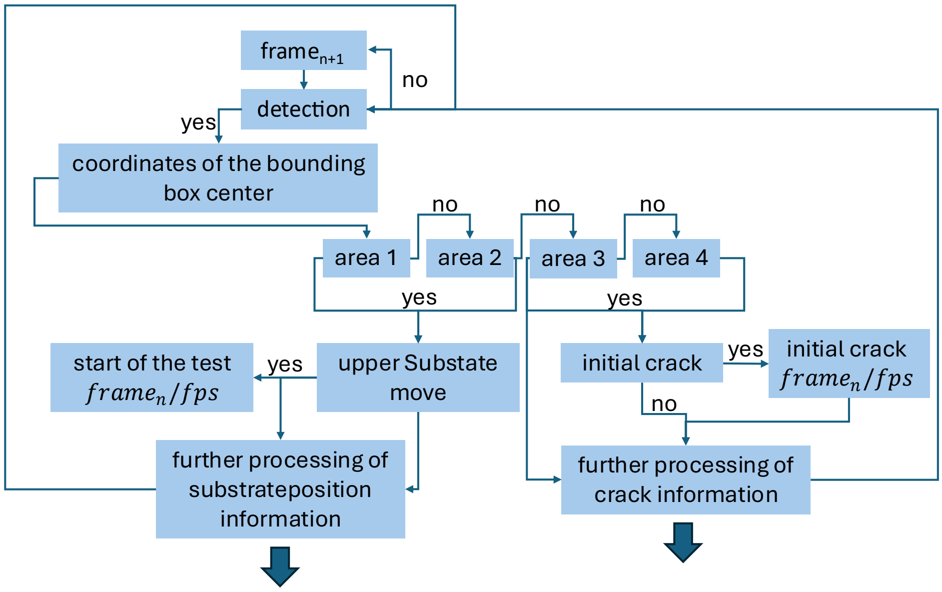

Fig. 7: Scheme of the Position and Experimental Information Cycle.

3.3. AI-Based Determination of Crack Geometry in Cyclic Tests

The automated evaluation of crack propagation in an SG joint is significantly complicated by the high deformability of the material, as illustrated in Fig. 8. A direct and realistic assessment of the actual crack extension is only possible in the unloaded state of the specimen, corresponding to the moment when the deformation in the test is zero. However, at this phase the deformation velocity reaches its maximum, resulting in motion blur, image distortion, and reduced accuracy of pixel-based feature extraction. In addition, in the closed state the crack is either not visible or appears only as a very thin line. At maximum deformation of the specimen, a sharp image can be captured due to the reversal of the loading direction. In this condition, however, the crack is in a mechanically distorted and opened state, meaning that the measured geometry does not correspond to the actual undeformed crack length. Furthermore, crack distortion leads to a shift of the crack maximum within the thick-layer adhesive joint. A simple back-calculation based solely on the test displacement to determine the crack tip position is not feasible, as this would require consideration of elastic and viscoelastic material deformations. Consequently, the actual crack propagation cannot be determined directly.

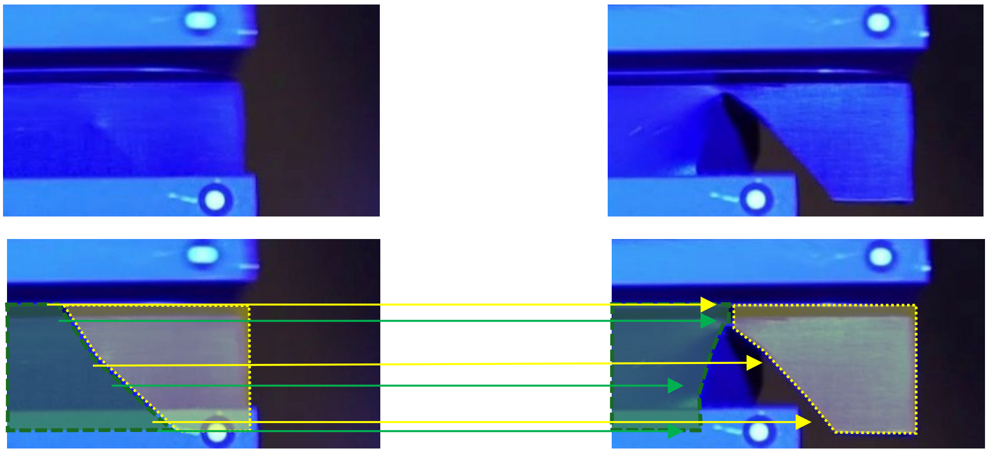

(a) (b)

Fig. 8: (a) Undeformed Crack; (b) Deformed Crack.

To enable quantitative evaluation despite deformation-induced image distortion, the detected crack geometry must be transformed back into an undeformed reference state. For this purpose, the determined deformation ratios of the upper and lower substrates are used to linearly map the pixel coordinates identified by segmentation to the zero-deformation state.

On this basis, the maximum crack growth can be determined independent of the respective deformation state as the geometric distance to the substrate. This makes it possible to quantify the damage level either as a percentage or, through pixel-to-length calibration, to convert it into real length units. Within the YOLO-based evaluation, the coordinates of the detected bounding boxes and segmentation masks can be exported and processed as x/y positions in image space. This enables mathematical post-processing of the geometric information during evaluation. Although YOLO primarily uses these coordinates for visualization of segmentations, detections, and bounding boxes, they simultaneously form the basis for further geometric calculations, taking known imaging reference dimensions into account.

In this study, Δx is determined from the coordinate displacement of the substrate bounding boxes. In addition, the bounding boxes provide information about the effective layer thickness of the silicone adhesive (Δy). When a crack is detected in the image, the segmentation mask allows direct geometric analysis of the crack shape. For example, the position of the left crack front (“Crack geometry information”) can be determined from the pixel with the maximum x-coordinate within the corresponding segmentation mask.

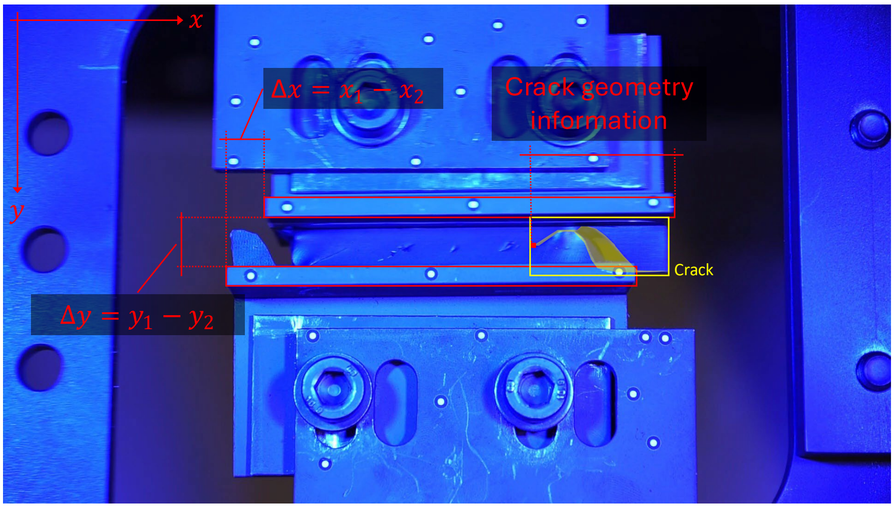

Fig. 9: Simplified Schematic Representation of Pixel-Based Information in the Image.

The geometric information extracted by the neural network is subsequently processed exclusively in a script-based manner. This involves a back-calculation of the detected crack geometry while accounting for the measured substrate deformation. The objective is to map the crack state observed at different deformation phases to a defined, undeformed reference state of the experiment. Through linear back-calculation, a fictitious undeformed state can be simulated. For this purpose, in each frame and for each pixel row, the segmentation mask is multiplied accordingly. The recalculation of the segmentation pixels is based on the relative deformation ratio between the substrates. From the resulting slope ratio, a linear positional correction of the pixel coordinates is applied depending on their location within the thick adhesive layer.

$$u = \frac{\Delta x}{\Delta y} * \left(y_{ls} - \prod_{i=1}^{H} i\right) \tag{2}$$

u	=	Shift
Δx	=	Difference in deformation relative to the zero crossing of the upper substrate
Δy	=	Difference between the lower and upper substrates
y_{ls}	=	y coordinate of the lower substrate
H	=	Image height resolution

In the following illustrations, all steps are presented in Fig. 10, which shows a short temporal sequence of the experiment over consecutive frames. The transformed segmentation pixels are displayed in red for visualization purposes. The green area represents the original crack segmentation mask identified by the artificial intelligence. The yellow area results from the visual overlap of the transformed (red) and original (green) segmentations and represents their intersection.

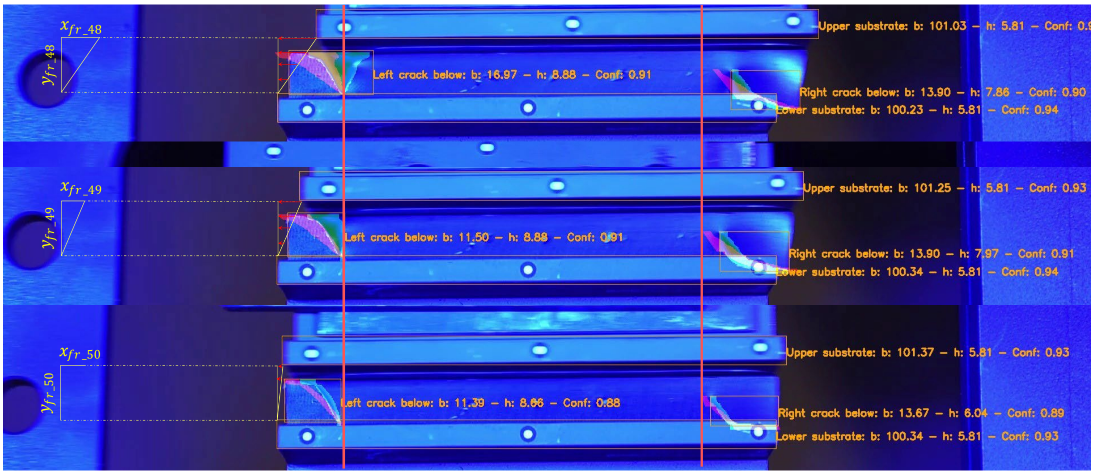

Fig. 10: Representation of a Short Section of the Experiment with Linear Back-Calculation.

3.4. Experimental Evaluation of AI-Based Crack Propagation Measurements

In the analysis of the crack geometries obtained from segmentation, sinusoidal fluctuations appear in the result curves due to cyclic deformation. The deformation-induced maxima and minima introduce a systematic uncertainty into the measurement methodology.

The following boundary conditions must be strictly considered when interpreting the measurement results and therefore define the methodological approach adopted in this work:

- The exact crack geometry is present at the zero-deformation crossing.
- At the zero-deformation crossing, image quality is at its worst due to the maximum deformation velocity.
- The best image quality is achieved at maximum deformation.
- Physical crack propagation is monotonically increasing and cannot exhibit a negative progression.
- At maximum deformation, the crack is present in a mechanically distorted geometry.

Considering these boundary conditions, crack propagation should preferably be determined in the range of minimal deformation, as the real crack geometry is present at this state. However, in this condition the detection reliability of the neural network is limited due to motion blur and the small crack opening width. Within the scope of this study, various criteria for defining the governing crack geometry were therefore investigated and compared with spot-check manual measurements from the video recordings. Initial evaluations indicate that determining crack propagation at the state of minimal segmentation area within the bounding box represents a suitable evaluation point. In this approach, the crack progression is captured in a minimally opened state and subsequently projected back to the closed reference state using the described back-calculation method for final evaluation.

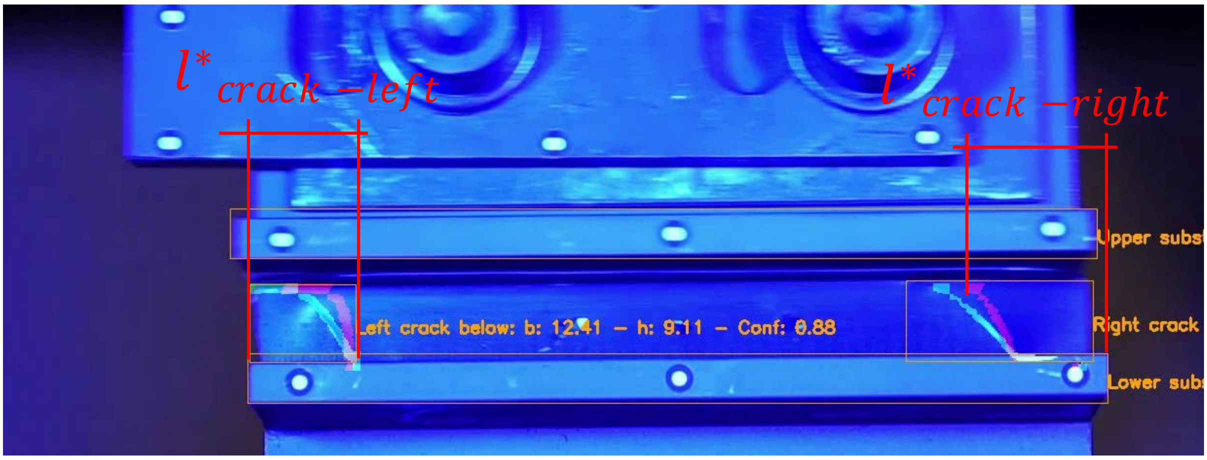

Fig. 11: Optimal Analysis Time Point.

The evaluation and comparison of the crack positions determined by the algorithm showed that a higher model input resolution of 2048 px can contribute to improved accuracy. This is particularly evident in the closer agreement with the manually determined normative crack lengths.

As illustrated in Figure 12a and Figure 12b, the manually measured values ($Left_{l*}\ ref, Right_{l*}\ ref, Comp_{l*}\ ref$) , $Comp_{l*}\ ref$ show significantly stronger convergence with the automatically determined analysis values of the neural network ($Left_{l*}\ AI, Right_{l*}\ AI, Comp_{l*}\ AI$) when a model with higher input resolution is used.

(a)

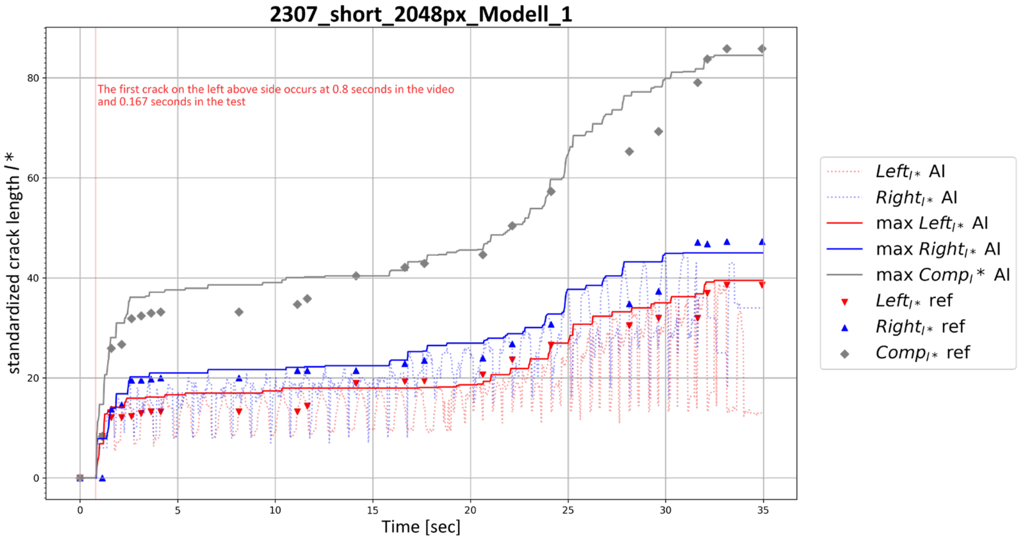

(b)

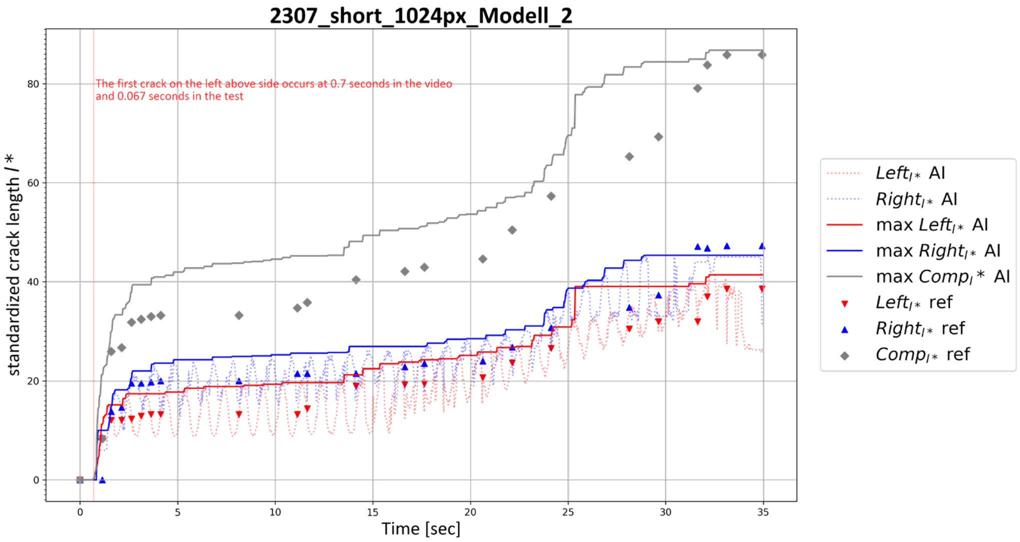

Fig. 12: (a) high model resolution (b) lower model resolution.

The relative errors Table 2 compared in to the manual reference measurements confirm the increased accuracy of the model when using a higher input resolution. However, it must be considered that the automated evaluation based on a neural network is subject to cycle-induced fluctuations. Since physical crack propagation is monotonic and can only assume increasing maximum values, short-term downward deviations must be interpreted as measurement- or detection-related artifacts. This characteristic is not explicitly accounted for in the tabulated representation and therefore leads to averaged deviations.

Table 2: Comparison of Measured Values.

Frame	Manual measurement		2307_short_2048px_Modell1		2307_short_1024px_Modell2		Rel. Error Comp	
	Left Crack	Right Crack	Left Crack	Right Crack	Left Crack	Right Crack	M1	M2
34	8.33	0	7.29	4.71	8.19	4.49	30.58	34.31
48	12.10	13.81	14.6	13.9	15.6	13.46	9.09	10.84
64	12.10	14.61	14.6	13.91	11.9	13.7	6.31	4.34
79	12.33	19.52	12.5	15.48	11.9	19.1	13.83	2.74
94	12.90	19.52	12.34	19.2	11.9	19.9	2.79	1.95
109	13.24	19.75	12.23	16.38	11.9	20.1	15.31	3.09
124	13.24	19.98	12.34	20.2	12.4	19.3	2.09	4.79
244	13.24	19.98	12.34	23.45	11.9	22.7	7.18	3.99
334	13.24	21.46	17.86	23.23	12.9	19.75	15.55	6.28
349	14.38	21.46	12.5	19.19	11.9	20.9	13.10	9.27
424	18.95	21.46	12.34	23.9	11.9	21.2	11.51	22.08
499	19.29	22.83	12.34	23.0	11.9	23.0	19.19	20.69
529	19.41	23.52	14.02	24.5	18.9	23.3	11.45	1.73
619	20.66	23.97	21.88	24.7	19.86	26.9	4.19	4.56
664	23.63	26.83	23.8	27.8	22.4	25.7	2.21	4.91
724	26.60	30.71	28.5	28.8	25.7	27.5	0.02	7.73
844	30.48	34.82	28.3	32.7	30.7	35.6	7.05	1.51
889	31.96	37.33	32.67	42.32	31.1	35.6	7.60	3.88
949	31.96	47.15	34.90	18.137	28.84	48.6	49.16	2.16
1048	36.99	46.80	12.12	11.78	24.6	41.6	250.59	26.57

In Fig. 13, different experimental series are compared to assess whether the accuracy and stability of the evaluation remain consistent and reproducible. The differing time axes in the analysis result from the video-based evaluation and merely indicate that the experiments started at different times, leading to temporally shifted crack initiation.

The results show a high level of agreement with the manual measurements, thereby confirming the applicability of the evaluation methodology based on a neural network.

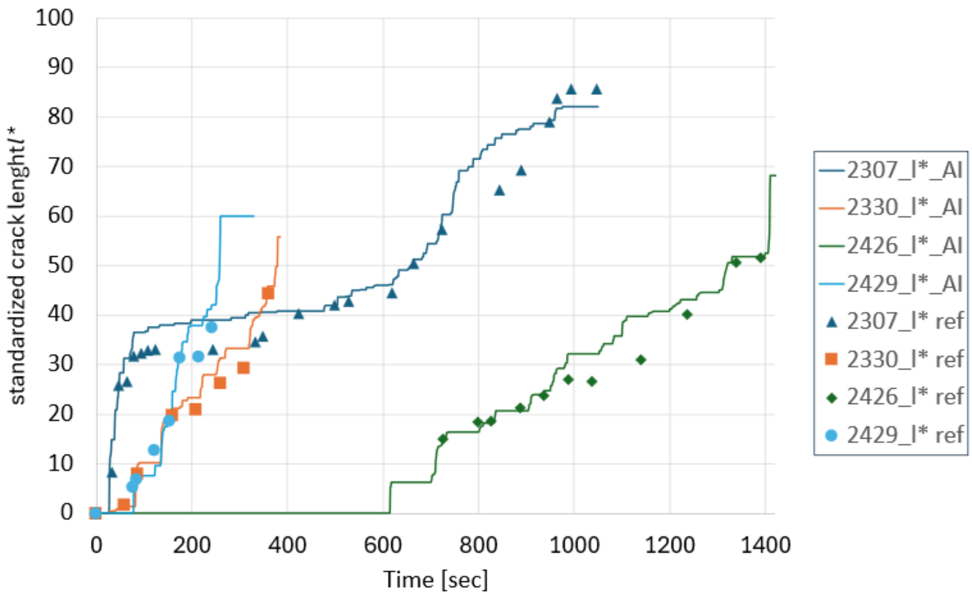

Fig. 13: Comparison of Different Experimental Series Using the Same Evaluation Methodology.

4. Conclusion and Evaluation

This study investigated whether automated crack propagation measurement using artificial intelligence is feasible. A network architecture primarily developed for object detection was selected to convert pixel-based image information into metrically evaluable quantities. The conducted investigations demonstrate significant potential for AI-based analysis of crack growth in cyclically loaded thick-layer adhesive joints. Within this work, image-based detection using neural networks was successfully integrated into an extended algorithmic evaluation framework, enabling the quantitative determination of relevant crack metrics.Crack distortion caused by cyclic deformation was transformed, in the minimally deformed state, into an undeformed reference condition through linear back-calculation, allowing the extraction of governing crack behavior parameters.

It was shown that a higher model input resolution improves agreement with manual reference measurements. Across multiple experimental series, the achieved results demonstrate reproducible accuracy, confirming the stability of the developed evaluation methodology. Future work will focus on further increasing accuracy, particularly by accounting for optical distortions and nonlinear deformation effects. Furthermore, alternative network architectures could improve applicability and robustness in future applications.

Regarding the performance of SG-joints under low-cycle fatigue performance, the proposed results in the paper enable a significant more detailed evaluation, considering the real crack length.

References

Bucak, Ömer, and Anneliese Hagl. 2006. 'Kleben im Bauwesen – gestern, heute, morgen – Allgemeine Übersicht und Ausblick auf die Forschung im Konstruktiven Glasbau an der Fachhochschule München (FHM)'. *Stahlbau* 75 (6): 499–507. https://doi.org/10.1002/stab.200610053.

Bues, Martin, Christian Schuler, Matthias Albiez, Thomas Ummenhofer, Holger Fricke, and Till Vallée. 2019. 'Load Bearing and Failure Behaviour of Adhesively Bonded Glass-Metal Joints in Façade Structures'. *The Journal of Adhesion* 95 (5–7): 653–74. https://doi.org/10.1080/00218464.2019.1570158.

Flotzinger, Johannes, Philipp J. Rösch, Christian Benz, et al. 2024. 'Dacl-Challenge: Semantic Segmentation during Visual Bridge Inspections'. *2024 IEEE/CVF Winter Conference on Applications of Computer Vision Workshops (WACVW)*, January 1, 716–25. https://doi.org/10.1109/WACVW60836.2024.00084.

Haghsheno, Shervin, Gerhard Satzger, Svenja Lauble, and Michael Vössing, eds. 2024. *Künstliche Intelligenz im Bauwesen: Grundlagen und Anwendungsfälle*. Springer Fachmedien Wiesbaden. https://doi.org/10.1007/978-3-658-42796-2.

Hagl, Anneliese. 2007. 'Bemessung von strukturellen Silikon-Klebungen'. *Stahlbau* 76 (8): 569–81. https://doi.org/10.1002/stab.200710060.

Huba, Antal, and Attila Bojtos. n.d. *Neue Methode zur Bestimmung des dynamischen Materialmodells von Silikongummi*.

Jahangir, Hashem, Harish Chandra Arora, José Viriato Araújo Dos Santos, Krishna Kumar, Aman Kumar, and Nishant Raj Kapoor, eds. 2025. *Damage Detection and Structural Health Monitoring of Concrete and Masonry Structures: Novel Techniques and Applications*. Springer Tracts in Civil Engineering. Springer Nature Singapore. https://doi.org/10.1007/978-981-97-8975-7.

Lee, Yunwoo, Heesoo Kim, Seongi Min, and Hyungchul Yoon. 2023. 'Structural Damage Detection Using Deep Learning and FE Model Updating Techniques'. *Scientific Reports* 13 (1): 18694. https://doi.org/10.1038/s41598-023-46141-9.

Lei, Jingsheng, Fu Lee Wang, Hepu Deng, and Duoqian Miao, eds. 2012. *Artificial Intelligence and Computational Intelligence: 4th International Conference, AICI 2012, Chengdu, China, October 26-28, 2012. Proceedings*. Vol. 7530, edited by David Hutchison, Takeo Kanade, Josef Kittler, et al. Lecture Notes in Computer Science. Springer Berlin Heidelberg. https://doi.org/10.1007/978-3-642-33478-8.

Müller, Paul, Christian Schuler, and Geralt Siebert. 2024. 'Experimental Investigations on the Cyclic Load-Bearing Behavior of Structural Glazing Joints under Seismic Load'. *Glass Structures & Engineering* 9 (3–4): 525–49. https://doi.org/10.1007/s40940-024-00273-0.

Müller, Paul, Christian Schuler, and Geralt Siebert. 2025a. 'Discussion of Failure Criteria and Low-Cycle Fatigue Performance of Structural Glazing Connections under Various Seismic Loading Scenarios'. *Construction and Building Materials* 471 (April): 140605. https://doi.org/10.1016/j.conbuildmat.2025.140605.

Müller, Paul, Christian Schuler, and Geralt Siebert. 2025b. 'Residual Performance of Structural Glazing Joints after Seismic Low-Cycle Fatigue Loading'. *Glass Structures & Engineering* 10 (3): 18. https://doi.org/10.1007/s40940-025-00303-5.

Paaß, Gerhard, and Dirk Hecker. 2020. *Künstliche Intelligenz: Was steckt hinter der Technologie der Zukunft?* Springer Fachmedien Wiesbaden. https://doi.org/10.1007/978-3-658-30211-5.

Roos, Eberhard, Karl Maile, and Michael Seidenfuß. 2022. *Werkstoffkunde für Ingenieure: Grundlagen, Anwendung, Prüfung*. Springer Berlin Heidelberg. https://doi.org/10.1007/978-3-662-64732-5.

Sonnet, Daniel. 2022. *Neuronale Netze kompakt: Vom Perceptron zum Deep Learning*. IT kompakt. Springer Fachmedien Wiesbaden. https://doi.org/10.1007/978-3-658-29081-8.

Wei, Chun, Xiaofei Hao, Chaoying Mao, Fachun Zhong, and Zhongping Liu. 2023. 'The Mechanical Properties of Silicone Rubber Composites with Shear Thickening Fluid Microcapsules'. *Polymers* 15 (12): 2704. https://doi.org/10.3390/polym15122704.

Challenging Glass Conference Proceedings – Volume 10 – June 2026 – Louter, Bos & Belis (Eds.)
International Conference on the Architectural and Structural Application of Glass
Challenging Glass Conference 10 – 15-17 June 2026 – TU Delft – The Netherlands

Platinum Sponsor

SAINT-GOBAIN

Gold Sponsors

EASTMAN

kuraray

NorthGlass

sedak

seele

Silver Sponsors

DOW

octatube

PERMASTEELISA GROUP

SEEN

Organisation

TU Delft

Technische Universität München

GHENT UNIVERSITY